MECHANICAL CHARACTERIZATION OF HARD PHASES BY MEANS OF NANOINDENTATION

F. Pöhl, A. Weddeling and W. Theisen

Ruhr-Universität Bochum; Chair of Materials Technology;
Universitätsstr. 150; Bochum; 44801; Germany

Keywords: Carbide, NbC, VC, TiC, WC, Nanoindentation, Mechanical Properties, Matrix Influence, Finite Element Method

Abstract

Hard phases are important features of wear-resistant materials. Hard metals and most tool steels thus consist of a high amount of hard phases, such as carbides and nitrides embedded in a softer metallic matrix. The mechanical properties and wear resistance of the system are controlled by the mechanical properties of the hard phases and the matrix. Since hard phases are brittle and have sizes in the range of microns, mechanical characterization with standard test methods, such as the tensile test, is often impossible. Nanoindentation, however, can be used to determine important mechanical parameters, such as hardness or Young's modulus, of brittle phases on a small scale. This paper deals with the mechanical characterization of different hard phases (NbC, VC, TiC, and WC) using nanoindentation. The measurements reveal significant differences in the mechanical properties and deformation behavior of the investigated phases. The deformation behavior was investigated using atomic force microscopy (AFM) and scanning electron microscopy (SEM) with energy-dispersive X-ray spectroscopy (EDS) analysis for the determination of chemical composition. The influence of the matrix on the indentation result of small hard phases embedded in a softer metallic matrix was evaluated using finite element method (FEM) simulations. These simulations give an insight into the complex deformation behavior during indentation of an embedded hard phase.

Introduction

Wear-resistant metallic materials often consist of hard phases (carbides, borides, nitrides) embedded in a softer metallic matrix [1]. The softer matrix supports the hard phases and ensures that the compound system has an adequate toughness. Due to their particular mechanical properties, monocarbides, such as NbC, VC, TiC, and WC are frequently used as reinforcement particles in tool steels and hard metals [2]. The wear behavior of these multiphase materials is essentially controlled by the mechanical properties, morphology, distribution, and dimensions of the hard phases [3]. Mechanical characterization of single phases in multiphase materials is thus crucial to understand the mechanical behavior of the compound and its wear resistance.

Mechanical testing, including handling and preparation, is not a trivial task on account of the small dimensions, in the order of microns, and the high hardness combined with the relatively low fracture toughness. This means that standard test methods, such as the tensile test, cannot be applied. In this respect, there is a lack of knowledge about the mechanical properties of hard

phases and particularly of carbides in tool steels and hard metals. The compound properties of these materials are usually characterized, rather than the properties of the individual phases [1].

One possible method that allows local mechanical characterization of small and brittle phases with minimum sample preparation is nanoindentation [1,4,5]. The results of these tests provide numerous important mechanical parameters, eg. hardness, Young's modulus or indentation energy. Furthermore, pile-up and sink-in characteristics around residual indentation imprints or induced cracks give insight into the complex deformation behavior of hard phases [4,6]. However, nanoindentation of small hard phases and the analysis of data are not trivial. Attention must be paid to the matrix influence on the indentation results [7]. In contrast to the exploration of substrate influence on the indentation results of coatings [8–10], a systematic investigation of the influence of the matrix on hard phase indentation is still missing. Size effects that are well-known from the indentation of metals can also significantly affect indentation results of hard phases [11].

This paper deals with the mechanical characterization of monocarbides in tool steels and in one hard metal by nanoindentation. It is shown that nanoindentation is a suitable method for the mechanical characterization of small scale, hard and brittle phases. However, attention must be paid to size effects and matrix influence on the indentation results. The objective of this study is, firstly, the mechanical characterization and measurement of important parameters of NbC, VC, TiC, and WC monocarbides, and secondly, the exploration of deformation behavior using scanning electron microscopy (SEM) and atomic force microscopy (AFM). A detailed insight into the mechanical behavior of monocarbides during indentation loading is given. These aspects are complemented by numerical and experimental investigations of the influence of the matrix on the indentation results from small embedded carbides.

Materials and Methods

Materials and Sample Preparation

The examined materials and phases are the NbC, VC, TiC, and WC monocarbides. NbC, VC, and TiC were investigated as features in tool steel matrices, whereas WC was evaluated as part of a hard metal.

The sample preparation for nanoindentation and microstructure analysis included grinding with SiC paper, followed by successive polishing with diamond suspensions with average grain sizes of 6, 3, and 1 µm. Final polishing was performed using an oxide polishing suspension with an average grain size of 0.25 µm.

Nanoindentation

Nanoindentation tests were conducted with a CSM Instruments' Nano-Hardness Tester (CSM NHT) indenter equipped with a Berkovich diamond tip. The indentation parameters are given in Table I. The maximum indentation depth for NbC, VC, and TiC was 400 nm. In comparison, WC shows a distinctly smaller particle size so that the indentation depth was adjusted to a maximum of 100 nm. In order to induce cracks, individual tests were conducted with a

maximum indentation depth (h_{max}) of 800 nm. The hardness and Young's modulus were calculated using the traditional Oliver and Pharr method [12,13]. In addition, the ratio between the elastic energy and the total indentation energy (W_{el}/W_{tot}) was determined. At least five load-displacement curves (P-h curves) were used to calculate the hardness, Young's modulus, and the W_{el}/W_{tot} ratio.

Table I. Nanoindentation Test Parameters

Indentation depth	**Loading/unloading rate**	**Dwell time at maximum depth**
100/400/800 nm	50 mN/min	10 s

Atomic Force Microscopy

In order to characterize the deformation behavior, the topography of the indents was measured with an atomic force microscope in the contact mode (Bruker type nano). The scanning speed was varied between 10 and 40 µm/s. Image Plus 2.9 software was used for data evaluation and three-dimensional visualization.

Scanning Electron Microscopy

Scanning electron microscopy (SEM) with energy-dispersive X-ray spectroscopy (EDS) analysis was used to characterize the microstructure, carbide morphology, residual indents, and chemical composition. The indentation of small scale NbC was analyzed with an SEM in-situ indentation module from Nanomechanics.

Finite-element Modelling (FEM)

FE calculations were performed using the FE software ABAQUS (version 6.11). The axisymmetric 2D FE model is based on prior work [7,14]. The geometry, mesh (detailed view), and boundary conditions of the model are shown in Figure 1. The indenter is modeled as an axisymmetric conical, rigid tip with an included half-apex angle $\theta = 70.3°$. A conical indenter with a half-apex angle of 70.3° leads to the same area-to-depth function as that of a Berkovich indenter. Numerous studies have shown that this approach sufficiently captures the response of a full-3D model [15–17]. Berkovich tips do not usually have ideal sharpness and show a tip rounding in the range of ~ 100 nm, which influences the P-h curve at shallow indentation depths [18]. The FE model took account of a typical tip rounding of 80 nm.

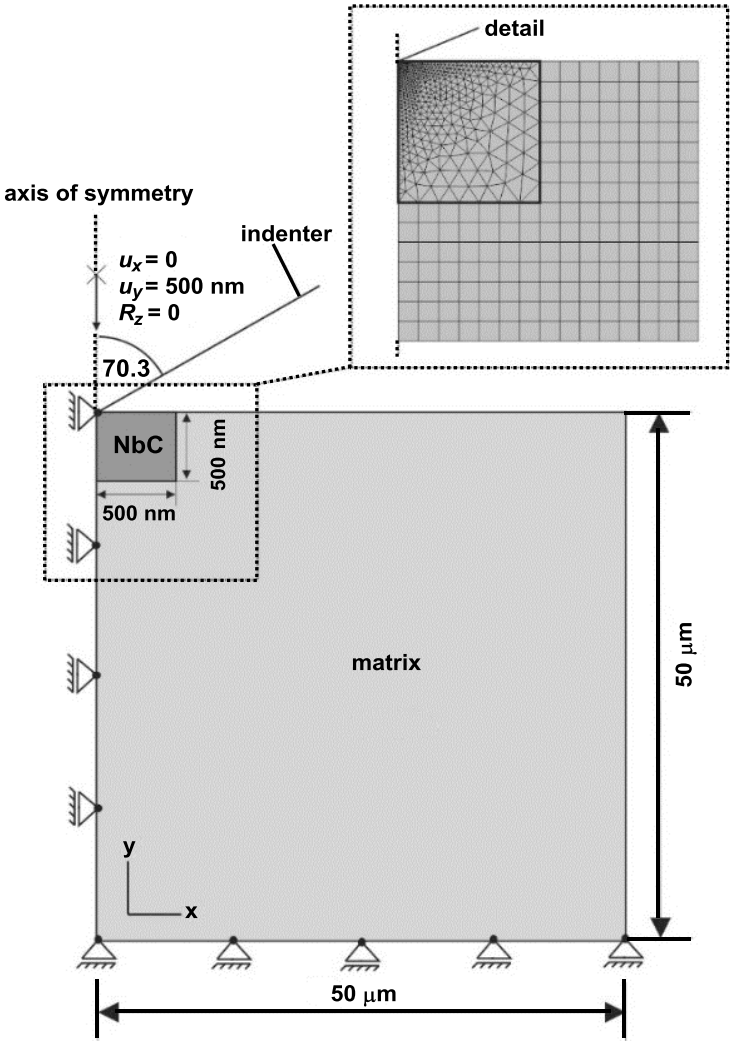

Figure 1. Schematic illustration of the geometry, mesh (detailed view), and boundary conditions of the FE model.

The domain has dimensions of 50 x 50 µm². It consists of a hard phase (NbC) embedded in a softer steel matrix. Since most investigated Nb carbides in this study have a blocky morphology, it is assumed to be rectangular. The dimensions are given in Figure 1. Simulations were carried out under displacement-control in which the indenter is pushed perpendicularly into the material with a maximum displacement u_y = 100 nm, Figure 1. All other degrees of freedom of the indenter are zero. The modeled sample is restricted by symmetry boundary conditions along the axis of symmetry and by floating supports along the lower edge. Contact between indenter and sample is assumed to be frictionless. Investigations have shown that the effect of friction can be neglected for the half-apex angle used in this study [19,20]. The area in close proximity to the point of contact is meshed finely with quad CAX3 elements with reduced integration and hourglass control. To minimize calculation effort, the fine mesh at the contact region is migrated to a coarse one consisting of quad CAX4R elements. The total number of elements is 25,424.

The elastic material behavior was modeled with Young's modulus E and Poisson's ratio ν. The J_2 von Mises flow theory was used to model plasticity [21]. The elasto-plastic material behavior of

the matrix is assumed to follow the Ludwik power law (Equation 1) with isotropic hardening and is described by three independent parameters: *K*, *n*, and *E* (Possion's ratio ν is assumed to be equal to 0.3 for the matrix and to be 0.27 for NbC) [5]. The Young's modulus of the matrix was assumed to be 210 GPa with a typical strain hardening exponent *n* of 0.2 [22,23]. The Young's modulus of NbC was assumed to be 400 GPa with no strain hardening ($n = 0$) [24]. This leaves only parameter *K* to be used for the FEM simulations.

$$\begin{aligned} \sigma &= E\varepsilon_{\mathrm{el}} \qquad \sigma \le \sigma_{\mathrm{y}} \\ \sigma &= K\varepsilon_{\mathrm{pl}}^{n} \qquad \sigma > \sigma_{\mathrm{y}} \end{aligned} \quad \text{and} \tag{1}$$

In order to determine the parameter *K*, the P-h curves of the matrix and a large NbC particle (no matrix influence) were determined. The P-h curves were then numerically calculated, and the material parameter *K* was adjusted until an agreement between experiment and simulation was achieved. The identified material parameters of the matrix and NbC are listed in Table II. The identified material parameters were used to establish the simulation of a compound consisting of a small NbC (edge length of 1 µm, see Figure 1) in a soft matrix. The numerical results were then compared to the experimental loading curve of a small embedded NbC.

Table II. Identified Material Parameters of the Steel Matrix and NbC for the FE Simulation

Phase	***K* (MPa)**	***n***	***E* (GPa)**	***v***
Steel matrix	4,250	0.2	210	0.30
NbC	22,500	0	400	0.27

Results

Figure 2 shows SEM images of the investigated materials. The NbC, VC, and TiC, with different morphologies and sizes are features of tool steels. They are embedded in a softer metallic steel matrix. The relatively large NbC particles have a blocky and square/triangular shape, whereas the large VC particles are spherical and the smaller TiC particles are spherical and curve shaped. The smallest investigated hard phase is WC, which is part of the microstructure of a cobalt-based hard metal.

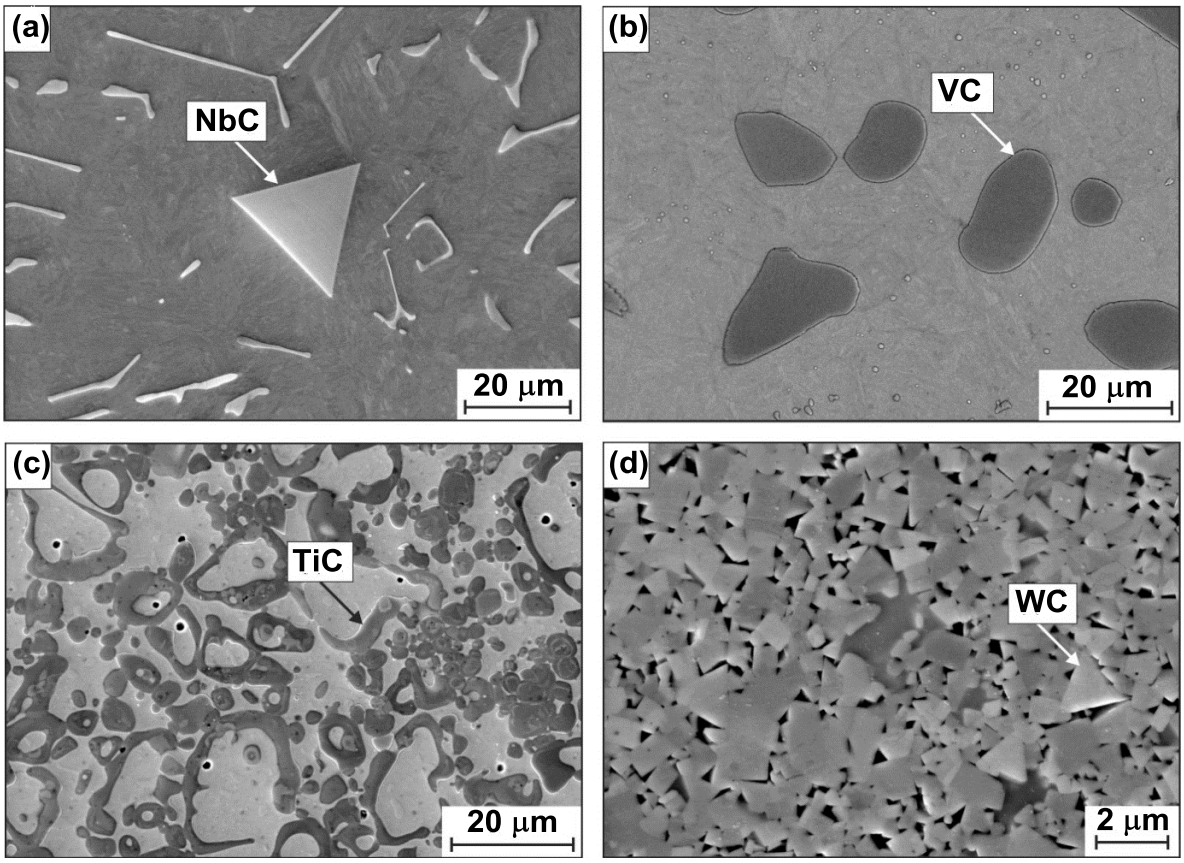

Figure 2. Metal-monocarbide microstructures; (a) Large blocky NbC in a tool steel matrix, (b) Large spherical VC in a tool steel, (c) Spherical and curve shaped TiC in a tool steel, (d) Small blocky WC in a hard metal with cobalt binder.

The chemical composition, measured by EDS, is listed in Tables III and IV. Although the measurement of carbon is not quantitative, the results illustrate that NbC and WC are relatively pure. In contrast, VC dissolves amounts of Fe and other alloying elements and TiC contains amounts of Fe, Mo, and Cr. Due to the presence of higher amounts of the elements Mo, Cr, W, Fe, and Nb, the VC corresponds more to a MC type, however, in this work it is declared as VC.

Table III. Chemical Composition in wt.% Measured by Energy-dispersive X-ray Spectroscopy Analysis. (Measurement of Carbon is not quantitative and is taken as the balance)

Phase	**Nb**	**V**	**Ti**	**W**	**C**	**Fe**	**Mo**	**Cr**
NbC	84.4	-	-	-	13.3	1.1	-	1.2
VC	3.2	52.4	2.6	7.2	14.5	2.5	13.3	4.3
TiC	-	-	74.0	-	18.9	1.6	4.6	0.9
WC	-	-	-	92.6	7.4	-	-	-

Table IV. Chemical Composition in Atomic % Measured by Energy-dispersive X-ray Spectroscopy Analysis. (Measurement of Carbon is not quantitative and is taken as the balance)

Phase	Nb	V	Ti	W	C	Fe	Mo	Cr
NbC	44.3	-	-	-	53.6	1.0	-	1.2
VC	1.3	36.3	2.1	1.5	46	1.7	5.3	3.3
TiC	-	-	48.2	-	48.9	0.9	1.5	0.6
WC	-	-	-	45.2	54.8	-	-	-

Representative P-h curves of the hard phases are given in Figure 3. Due to the small size of the WC particles, the maximum indentation depth was set to 100 nm. The curves for all the hard phases are similar in shape and show a high amount of elastic recovery during unloading. It is known that fracture during indentation testing can cause pop-in events during loading (plateaus in the loading curve) [25]. However, the loading curves are smooth and do not show indications of brittle cracking.

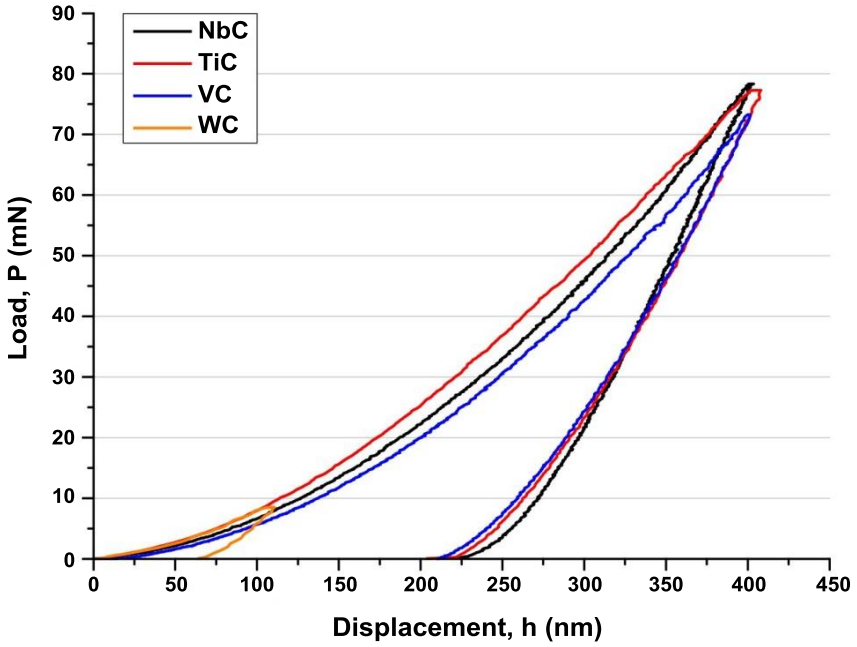

Figure 3. Mean P-h curves of the investigated hard phases.

The calculated mechanical parameters of the hard phases are summarized in Table V. The indentation hardness of all the carbides is within a similar range between 29.5 GPa and 32 GPa. The highest hardness was found for NbC, followed by VC, TiC, and WC. Another important mechanical parameter in indentation testing is the elastic energy to total indentation energy ratio (W_{el}/W_{tot}). The W_{el}/W_{tot} ratios for NbC, VC, and TiC are comparable with high values between 50 and 57%. In contrast, WC shows a distinctly lower ratio of 37%. A comparison of hardness and W_{el}/W_{tot} ratio is given in Figure 4.

Table V. Mechanical Parameters Measured by Nanoindentation. Indentation Hardness H_i was Converted to a Vickers Hardness Number (HV) According to DIN EN ISO 14577 ($HV = 92.62 \cdot H_i$ in GPa), Although the Indentation Depth h was <6 µm [26]

Phase	**H_i (GPa)**	**HV**	***E* (GPa)**	**W_{el}/W_{tot}**
NbC	32.0 ± 3.8	2964 ± 352	431 ± 36	54 ± 4
VC	30.7 ± 2.0	2845 ± 182	423 ± 20	50 ± 3
TiC	29.7 ± 2.5	2763 ± 227	392 ± 26	57 ± 5
WC	29.5 ± 3.3	2672 ± 302	675 ± 44	37 ± 3

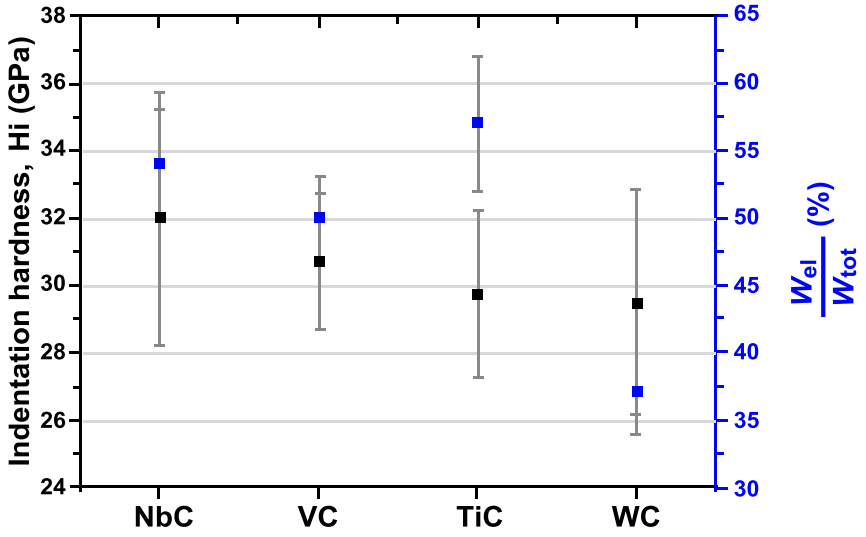

Figure 4. Comparison of hardness and W_{el}/W_{tot} ratio.

Size effects can significantly influence the indentation results of materials. In the case of self-similar indenters (eg. Berkovich), the indentation size effect (ISE) leads to an increase in measured strength with decreasing indentation depth. The ISE for self-similar indenters is characterized by measuring the hardness as a function of indentation depth [27]. Another way to detect an increase in strength with decreasing indentation depth is the analysis of the loading curvature C (related to Martens hardness). The loading curvature is dependent on the indenter geometry and the mechanical properties (strength) of the investigated material. For an ideal self-similar indenter and a homogeneous material without ISE, the loading curvature is constant and is given by Equation 2. In the case of ISE, the loading curvature is a function of indentation depth h and increases with decreasing h, which is caused by an increase in strength (Equation 3) [14].

$$P = Ch^2 \quad \text{with} \quad C = \text{const.} \tag{2}$$

$$P = Ch^2 \quad \text{with} \quad C = f(h) \tag{3}$$

The parameter C is plotted as a function of indentation depth in Figure 5. It increases with decreasing indentation depth h for all hard phases. The phases NbC, TiC, and WC show a similar and distinct increase in C. In contrast, the increase is considerably lower for VC.

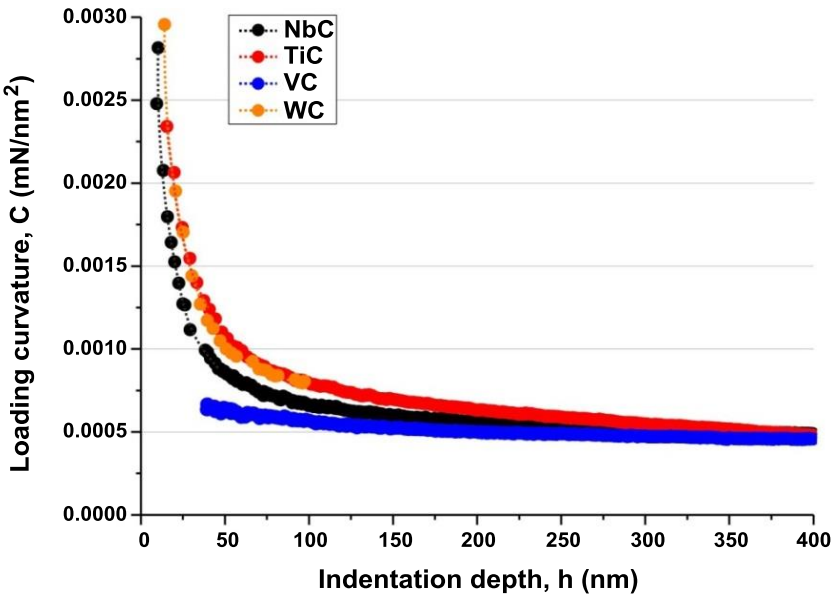

Figure 5. Increase of loading curvature C (related to strength) with decreasing indentation depth.

Figure 6 and Figure 7 illustrate the deformation behavior of NbC, VC, and TiC. The indentation imprints in WC are too shallow for an accurate analysis due to the low indentation depth and high elastic rebound during unloading. As can be seen in Figure 6(b) and 6(c), the indentation in VC and TiC causes fracture, with induced cracks at the edges and corners of the imprint. The deformation of TiC also shows the formation of discrete deformation bands. An example is given in Figure 6(d). In contrast, these observations were not found for NbC. From Figure 6(a) it is evident that there are no cracks or discrete deformation bands. The difference in deformation behavior (fracturing) between VC and NbC is also illustrated in Figure 7.

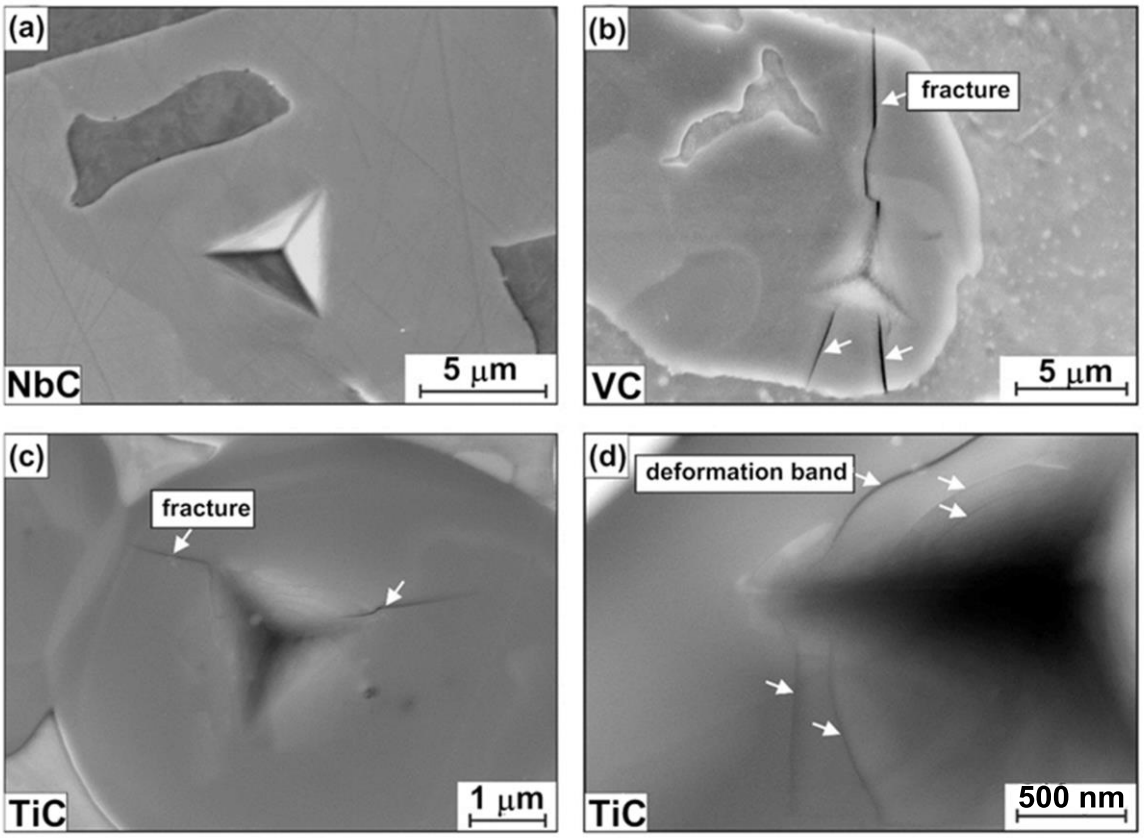

Figure 6. Deformation and fracture of; (a) NbC, (b) VC, (c) and (d) TiC.

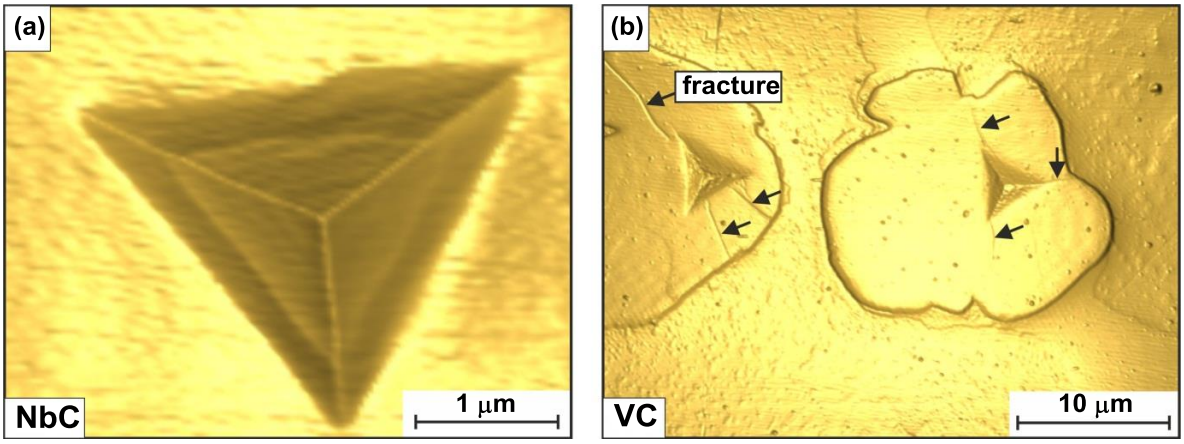

Figure 7. Topographic images of residual indentation imprints in; (a) NbC and (b) VC.

Topographic images of the imprints reveal that all investigated hard phases exhibit slight sink-in around the indentation, rather than pile-up. An example, including a height profile across an imprint, is given for NbC in Figure 8.

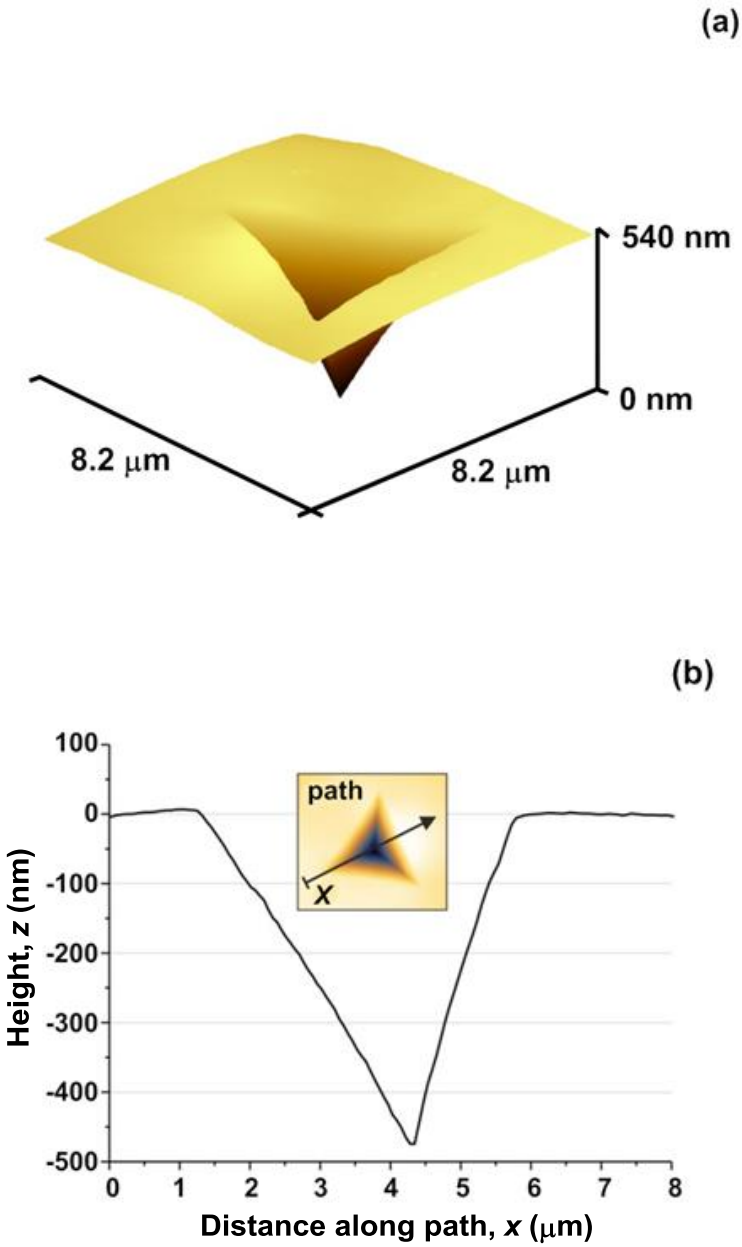

Figure 8. (a) 3D image of an imprint in NbC (h_{max} = 800 nm) and (b) height profile along path *x*.

Another factor influencing the indentation results from an embedded hard phase is the surrounding matrix. As can easily be recognized in Figure 9, the indentation of small hard phases can lead to deformation of both the hard phase and the matrix. Thus, the P-h curve, as well as the calculated hardness, Young's modulus and W_{el}/W_{tot} ratio can be significantly affected by the matrix. However, indications of an influence of the matrix in a measured P-h curve cannot easily be detected.

In order to illustrate the matrix influence, the measured loading parts of the P-h curve for a large and a small NbC, as well as the pure matrix are plotted in Figure 10. At low indentation depths,

the loading curves of a small and a large NbC are in good agreement. At a depth of approximately 42 nm, the softer matrix begins to influence the P-h curve for the smaller NbC particle by shifting it to lower forces with increasing indentation depth. Lower forces are accompanied by a reduction in the measured strength (lower hardness and W_{el}/W_{tot} ratio). FEM simulations prove that the measured curve for the small NbC particle is significantly influenced by the softer matrix. The data points in Figure 10 are the results of FEM simulations that illustrate the force shift caused by the matrix influence. Due to the matrix influence, the loading curvature C of small NbC particles (rectangular 500 nm x 1000 nm) is reduced by ~ 18% at an indentation depth of 100 nm, Figure 11. This clearly shows the underestimation of strength as a result of matrix deformation. The von Mises stress distribution of the compound system (small NbC and matrix) at the maximum indentation depth (100 nm) clearly reveals matrix deformation that influences the P-h curve, Figure 12.

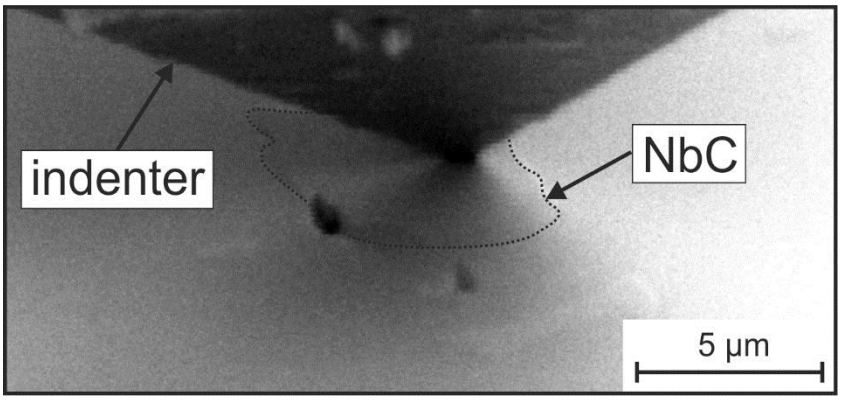

Figure 9. Indenter in contact with small NbC embedded in steel matrix.

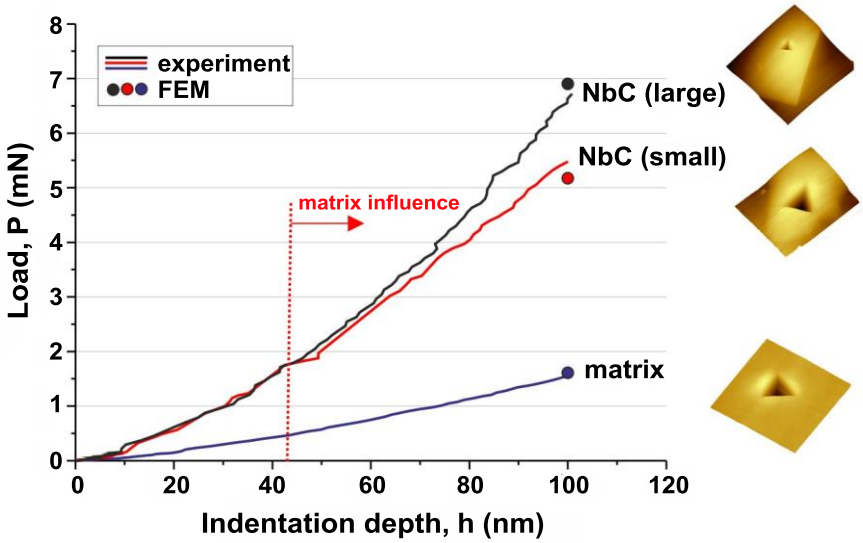

Figure 10. Experimental loading curves (solid lines) and results of FEM simulations (points) for a large NbC and a small embedded NbC, as well as the pure steel matrix. At indentation depths of approximately 42 nm and above, the matrix influences the indentation results from the small embedded NbC.

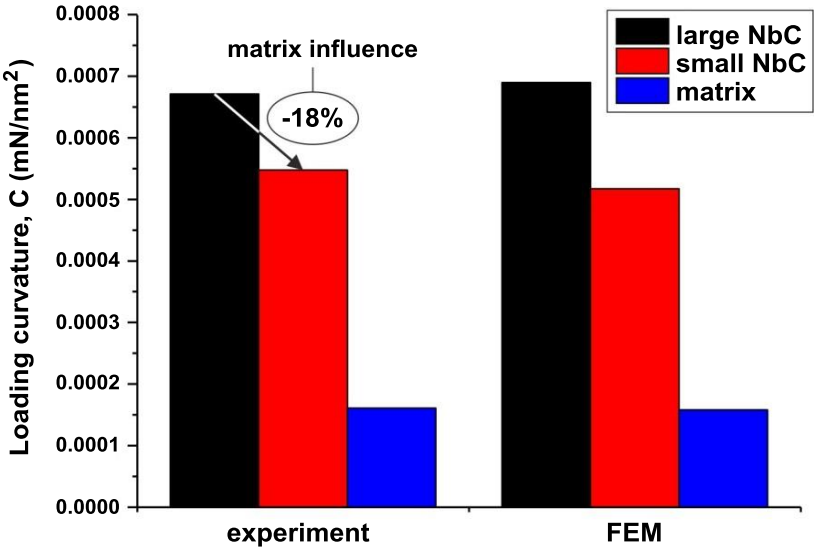

Figure 11. Comparison of loading curvature C of large NbC and small embedded NbC, as well as the pure matrix. The matrix influence leads to a reduction of 18% for the small NbC. The maximum indentation depth is 100 nm.

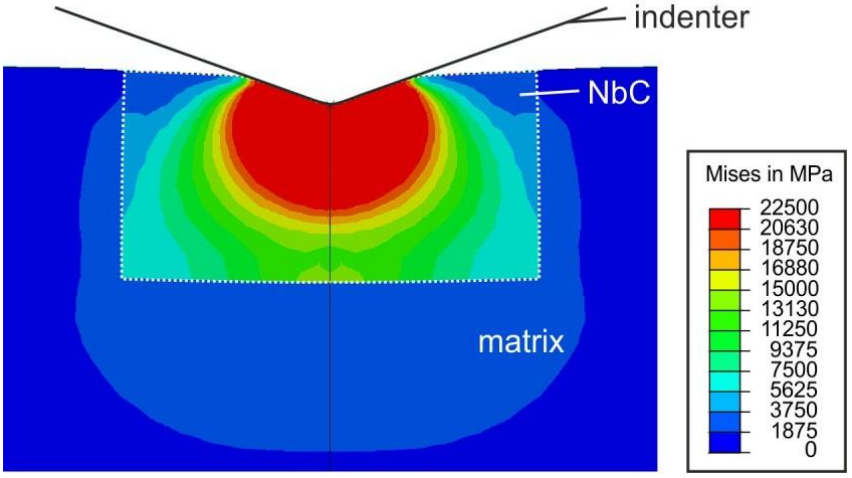

Figure 12. Numerically calculated von Mises stress distribution in small embedded NbC and the surrounding matrix. Deformation takes place in the NbC and in the matrix.

Discussion

The compound wear resistance of multiphase materials is dependent on the microstructure (including the single-phase mechanical properties) and the wear system [28]. In order to improve the abrasive wear resistance, microstructures often consist of high amounts of hard phases embedded in a softer metallic matrix.

It has often been shown that hard phases, as features in wear-resistant materials, need to be harder than the abrading particles in order to be effective [28]. One important property directly related to the abrasive wear resistance of the compound is thus the hardness of the hard phase. All investigated hard phases (NbC, TiC, VC, and WC) exhibit a high hardness in the range between 29.5 GPa and 32 GPa. Due to their hardness, which is higher than most abrading particles/minerals, these carbides are useful as reinforcement particles in wear-resistant materials. The highest measured hardness was found for NbC, followed by VC, TiC, and WC.

Variations of chemical composition of the monocarbides can lead to changes in stoichiometry and atomic bonding, which can significantly affect the mechanical properties. Hill et al. revealed a negative influence of Mo present in TiC [29]. In their investigations, the diffusion of Mo into the TiC led to a reduction of the hardness. The TiC and VC investigated in this study also contain Mo along with other alloying elements. In contrast, NbC and WC are relatively pure and do not dissolve high amounts of alloying elements. Negative influences caused by diffusion of alloying elements into NbC and WC can thus be excluded. Furthermore, Cr depletion of a corrosion-resistant matrix cannot occur with NbC and WC.

As is well-known from metallic materials, the indentation size effect (ISE) can significantly affect indentation results [27]. According to Nix and Gao, the ISE is usually related to the density of the geometrically necessary dislocations, which are dependent on material and indenter geometry. In the case of self-similar indenters, (eg. Berkovich), the ISE is a size-dependent increase in measured strength (hardness) with decreasing indentation depth [30]. Similar to metallic materials, an ISE was also observed for oxides and carbides [12]. Bull et al. related the ISE of ceramics to discrete deformation effects. They concluded that the deformation of hard phases takes place in discrete bands rather than being continuous [31,32]. A similar behavior can be seen in Figure 6(d).

Figure 5 reveals that all investigated monocarbides exhibit an ISE. It is related to discrete deformation effects with a size-dependent increase in measured strength. The ISE becomes apparent by an increase in C (loading curvature) with decreasing indentation depth h. The phases NbC, TiC, and WC show a similar ISE consisting of a distinct increase in C. In contrast, the ISE of VC is considerably lower. The hardness of WC was measured with a maximum indentation depth of 100 nm, but with a maximum indentation depth of 400 nm for all the other carbides. As Figure 5 clearly illustrates, the ISE in WC is still present at an indentation depth of 100 nm. Due to the small particle size of WC, it was not possible to increase the indentation depth without causing a significant matrix influence on the measurement, however, it can be expected that the hardness of WC measured with an indentation depth of 400 nm would be considerably lower than 29.5 GPa (equivalent to 2672 HV). Berns and Franco measured a Vickers hardness number for WC (1914 HV 0.05) at a higher indentation depth which is considerably lower [5]. It is thus concluded that the hardness of NbC, TiC, and VC is significantly higher than the hardness of WC. However, the investigations show that care must be taken when comparing the hardness of hard phases measured at different indentation depths.

Another important indentation parameter is the W_{el}/W_{tot} ratio. Niederhofer and Huth showed that the W_{el}/W_{tot} ratio is a potentially useful parameter which can be related to the wear behavior [33]. All monocarbides show a high amount of elastic recovery during unloading, which is typical for

hard phases. The W_{el}/W_{tot} ratio of NbC, TiC, and VC is considerably higher (50-57%) compared to WC (37%). Based on the investigations of Niederhofer and Huth, it is concluded that a high W_{el}/W_{tot} ratio might be beneficial for increasing the wear resistance, however, a systematic investigation has not yet been conducted.

Along with the hardness and the W_{el}/W_{tot} ratio, the fracture toughness has a crucial influence on the wear behavior. The deformation and cracking behavior of hard phases during indentation is related to the fracture toughness and to the mechanical behavior under wear attack. The indentation imprints in NbC feature a homogeneous deformation without fracture and cracking. Despite having a high W_{el}/W_{tot} ratio, the deformation is relatively ductile. At equal indentation depth (800 nm), TiC and VC show cracking. Furthermore, discrete deformation bands are observed for TiC, Figure 6. As a consequence, TiC and VC are likely to have lower fracture toughness than NbC. Due to the small phase sizes, the cracks (ending at the phase boundary) could not be analyzed in order to estimate the fracture toughness with empirical equations. Another aspect of the deformation behavior is the slight sink-in tendency around indentation imprints. Sink-in is usually observed for metallic materials with a high work-hardening potential, but is also related to the W_{el}/W_{tot} ratio [34]. It is concluded that the monocarbides do not exhibit significant work hardening and the slight sink-in is solely caused by the high elastic deformation component.

An important effect on the indentation results of embedded hard phases is exerted by the surrounding matrix. FEM simulations illustrate that the indentation of a hard phase can lead to the deformation of both the hard phase and the softer matrix, Figure 12. The deformation of a softer matrix affects the P-h curve by shifting the loading curve to lower forces. This leads to a lower measured hardness. The indentation of a small rectangular NbC particle (1000 nm x 500 nm) embedded in a steel matrix leads to a significant matrix influence at a depth of 42 nm and above, Figure 11. Measurements at shallow indentation depths may become inaccurate due to the ISE, indenter tip rounding, surface roughness, etc.

In summary, NbC, TiC, VC, and WC monocarbides have a high hardness and a high W_{el}/W_{tot} ratio. Both parameters are considered to be beneficial for improving the wear resistance. Taking into consideration the ISE, WC shows the smallest hardness and W_{el}/W_{tot} ratio. NbC is likely to have the highest toughness (no cracks and deformation bands), although it has the highest hardness. Furthermore, NbC is relatively pure and does not dissolve high amounts of alloying elements that could exert a negative influence on the mechanical properties or lead to Cr depletion of the corrosion-resistant steel matrix.

Conclusions

The main conclusions from this study are:

1. The NbC, TiC, VC, and WC monocarbides have a high hardness and a high W_{el}/W_{tot} ratio. Both are considered to be beneficial for improving wear resistance.

2. The TiC and VC investigated in this study contain Fe and other alloying elements. In contrast, NbC and WC are relatively pure and do not dissolve high amounts of alloying

elements. Negative influences caused by diffusion of alloying elements into NbC and WC can thus be excluded.

3. All investigated hard phases show a distinct ISE that is related to discrete deformation effects with a size-dependent increase in measured strength. The ISE leads to a higher measured hardness with decreasing indentation depth (Berkovich indenter). Due to the small indentation depth of 100 nm, the hardness of WC is higher than values reported in the literature [5]. It is concluded that the hardness of NbC, TiC, and VC is significantly higher than that of WC at a given indentation depth.

4. The indentation imprints in NbC feature homogeneous deformation without fracture and cracking. The W_{el}/W_{tot} ratio is high, whereas the deformation is relatively ductile. In contrast, TiC and VC exhibit cracking at equal indentation depth (800 nm). Furthermore, discrete deformation bands are observed for TiC. As a consequence, TiC and VC are likely to have a lower fracture toughness than NbC.

5. FEM simulations illustrate that the indentation of a small hard phase can lead to the deformation of both the hard phase and the softer matrix. Deformation of the softer matrix affects the P-h curve by shifting the loading curve to lower forces. This leads to a lower measured hardness and Young's modulus.

Acknowledgements

The authors gratefully acknowledge financial support by the Deutsche Forschungsgemeinschaft (project HU 1882/1-1).

References

1. H. Berns, "Microstructural Properties of Wear-resistant Alloys," *Wear,* 1995, no. 181-183:271-279.

2. S. Huang et al., "Microstructural Properties of Wear-resistant Alloys," *International Journal of Refractory Metals and Hard Materials*, 2015, no. 48:418-426.

3. N. Axén and K. Zum Gahr, "Wear of TaC and TiC Steel Composite Hardfacings by Soft and Hard Abrasives," *Materialwissenschaft und Werkstofftechnik*, 23 (10) (1992), 360-367.

4. D. Casellas et al., "Fracture Toughness of Carbides in Tool Steels Evaluated by Nanoindentation," *Acta Materialia*, 2007, no. 55:4277-4286.

5. H. Berns and S. Franco, "Properties of Hard Particles at Room Temperature and Elevated Temperature," *Proceedings of III Seminário Brasileiro* (1994).

6. J. Alcalá, A. Barone and M. Anglada, "The Influence of Plastic Hardening on Surface Deformation Modes Around Vickers and Spherical Indents," *Acta Materialia,* 2000, 48:3451-3464.

7. F. Pöhl, S. Huth and W. Theisen, "Finite Element Method-assisted Acquisition of the Matrix Influence on the Indentation Results of an Embedded Hard Phase," *Materials Science and Engineering: A*, 2013, 559:822-828.

8. N. Sakharova et al., "On the Determination of the Film Hardness in Hard Film/Substrate Composites Using Depth-sensing Indentation," *Ceramics International*, 2013, 39:6251-6263.

9. C. Gamonpilas and E. Busso, "On the Effect of Substrate Properties on the Indentation Behaviour of Coated Systems," *Materials Science and Engineering: A*, 2004, 380:52-61.

10. J. Antunes et al., "On the Determination of the Young's Modulus of Thin Films Using Indentation Tests," *International Journal of Solids and Structures*, 2007, 44:8313-8334.

11. Y. Milman, A. Golumbenko and S. Dub, "Indentation Size Effect in Nanohardness," *Acta Materialia*, 2011, 59:7480-7487.

12. W. Oliver and G. Pharr, "An Improved Technique for Determination Hardness and Elastic-modulus Using Load and Displacement Sensing Indentation Experiments," *Journal of Materials Research*, 1992, 7:1564-1583.

13. W. Oliver and G. Pharr, "Measurement of Hardness and Elastic Modulus by Instrumented Indentation: Advances in Understanding and Refinements to Methodology," *Journal of Materials Research*, 2004, 19:3-20.

14. F. Pöhl and W. Theisen, "Indentation of Self-similar Indenters: An FEM-assisted Energy-based Analysis," *Journal of the Mechanics and Physics of Solids*, 2014, 66:32-41.

15 K. Johnson, "The Correlation of Indentation Experiments," *Journal of the Mechanics and Physics of Solids*, 1970, 18:115-126.

16. P. Larsson, "Modelling of Sharp Indentation Experiments: Some Fundamental Issues," *Philosophical Magazine* 86 (33-35) (2006), 5155-5177.

17. N. Sakharova et al., "Comparison between Berkovich, Vickers and Conical Indentation Tests: A Three-dimensional Numerical Simulation Study," *International Journal of Solids and Structures*, 2009, 46:1095-1104.

18. A. Warren and Y. Guo, "Machined Surface Properties Determined by Nanoindentation: Experimental and FEA Studies on the Effects of Surface Integrity and Tip Geometry," *Surface & Coatings Technology*, 2006, 201:423-433.

19. M. Mata and J. Alcalá, "The Role of Friction on Sharp Indentation," *Journal of the Mechanics and Physics of Solids*, 2004, 52:145-165.

20. J. Bucaille et al., "Determination of Plastic Properties of Metals by Instrumented Indentation Using Different Sharp Indenters," *Acta Materialia*, 2003, 51:1663-1678.

21. ABAQUS (2009) User's Manual v. 6.9, ABAQUS Inc. Providence, USA.

22. M. Le, "Materials Characterisation by Dual Sharp Indenters," *International Journal of Solids and Structures*, 2009, 46:2988-2998.

23. X. Chen et al., "On the Uniqueness of Measuring Elasto-plastic Properties from Indentation: The Indistinguishable Mystical Materials," *Journal of the Mechanics and Physics of Solids*, 2007, 55:1618-1660.

24. X. Jiang and J. Zhao, "Correlation between Hardness and Elastic Moduli of the Covalent Crystals," *Computational Materials Science*, 2011, 50:2287-2290.

25. K. Fu et al., "Analysis on Cracking in Hard Thin Films on a Soft Substrate under Berkovich Indentation," *Vacuum*, 2015, 112:29-32.

26. DIN EN ISO 14577 (2012) Instrumentierte Eindringprüfung zur Bestimmung der Härte und anderer Werkstoffparameter.

27. G. Pharr, E. Herbert and Y. Gao, "The Indentation Size Effect: A Critical Examination of Experimental Observations and Mechanistic Interpretations," *Annual Review of Materials Research*, 2010, 40:271-292.

28. H. Berns, "Hard Alloys - Microstructure and Abrasion Resistance," *Proceedings of the III Brazilian Seminar on Wear Resistant Materials*, (1994), Fortaleza, Brasil.

29. H. Hill et al., "The Impact of Processing on Microstructure, Single-phase Properties and Wear Resistance of MMCs," *Wear*, 271 (9-10) (2011), 1895-1902.

30. W. Nix and H. Gao, "Indentation Size Effects in Crystalline Materials: A Law for Strain Gradient Plasticity," *Journal of the Mechanics and Physics of Solids*, 46 (3) (1998), 411-425.

31. S. Bull, "On the Origins and Mechanisms of the Indentation Size Effect," Zeitschrift für Metallkunde, 94 (7) (2003), 787-792.

32. S. Bull, T. Page and E. Yoffe, "An Explanation of the Indentation Size Effect in Ceramics," *Philosophical Magazine*, 59 (6) (1989), 281-288.

33. P. Niederhofer and S. Huth, "Cavitation Erosion Resistance of High Interstitial CrMnCN Austenitic Stainless Steels," *Wear*, 301 (1-2) (2013), 457-466.

34. G. Das, S. Gosh and R. Gosh, "Materials Characterization and Classification on the Basis of Materials Pile-up Surrounding the Indentation," *Materials Science and Engineering: A*, 2005, 408:158-164.